RESEARCH ARTICLE

Remote Vital Signs Measurement of Indoor Walking Persons Using mm-Wave FMCW Radar

YAOKUN HU[1,2] **AND TAKESHI TODA**[3]

[1]Graduate School of Science and Technology, Nihon University, Tokyo 101-0062, Japan
[2]Fujitsu Ltd., Kawasaki 211-0053, Japan
[3]College of Science and Technology, Nihon University, Tokyo 101-0062, Japan

Corresponding author: Yaokun Hu (csgy19014@g.nihon-u.ac.jp)

ABSTRACT Research on radar-based non-contact vital sign monitoring systems is critical during the COVID-19 epidemic. The accuracy of remote vital sign measurements has increased with the advancement of radar technology and various algorithms. Most studies require subjects to remain stationary, such as standing, sitting in a chair, or lying on a bed, and various measurement algorithms have been proposed. However, maintaining a stationary state as a prerequisite for measurement limits the development and application prospects of radar-based vital sign monitoring systems. Therefore, this paper presents a novel method for monitoring the vital signs of moving targets using a millimeter-wave frequency-modulated continuous-wave (FMCW) radar. The experimental results showed that regardless of whether the subjects walked at 1 m/s or with the left side of their body facing the radar, the accuracy of the heart rate measurement remained high. In the fixed-route experiments, the root mean squared error (RMSE) for heart rate estimation was 4.09 bpm, with an accuracy of 95.88%.

INDEX TERMS FMCW radar, health care, heart rate, ICEEMDAN, radar signal processing, remote sensing, vital signs.

I. INTRODUCTION

The COVID-19 epidemic is currently sweeping the world, and in order to reduce the rate of infection, contactless products are gaining popularity and are being used in a large number of ways in everyday life. Examples are remote temperature measurement, automatic finger sanitizers, remote office software, remote vital signs detection, and many other applications. This study proposes a novel solution for radar-based non-contact vital sign measurements.

Physiological parameters, such as respiration, heart rate, body temperature, and blood pressure, are essential in biomedicine because physiological data can often reveal a person's health. Respiratory and heart rate signals are important parameters for determining whether the activity of the human heart and lungs is normal. The activity of the human

heart and lungs directly influences the activity of various organs and muscles. With the advancement of biomedical technology in recent years, an increasing number of methods have been developed for detecting respiration and heartbeat signals. Electrocardiography (ECG), finger pressure pulse measurement, photoplethysmography (PPG), and phonocardiography are the most commonly used methods [1]–[3]. However, these detection methods are essentially contact measurement methods that require electrodes or sensors to contact the person being measured. These methods are inconvenient for epidemiological testing or monitoring the vital signs of isolated persons [4]–[6]. Therefore, during the COVID-19 epidemic, research into radar-based non-contact vital sign monitoring systems is critical.

In [7], the authors proposed a radar-based measurement method for estimating the heart rate of a single subject when multiple experimental subjects. In [8], they used a frequency-modulated continuous-wave (FMCW) radar to measure a

The associate editor coordinating the review of this manuscript and approving it for publication was Wei Wang.

person's vital signs while lying in bed. In [9], a vital sign estimation method based on permutation entropy and the ensemble empirical mode decomposition (EEMD) algorithm was proposed for ultra-wideband (UWB) radar. In most radar-based vital sign estimation studies, subjects were required to remain stationary, such as standing, sitting on a chair, or lying on a bed [7]–[14]. This facilitated the acquisition of displacement signals from the skin of the subject's body, which improved the measurement accuracy. However, maintaining a stationary state as a prerequisite for measurement limits the development and application prospects of radar-based vital-sign monitoring systems. Therefore, there is a critical need for a method that can accurately measure the vital signs of moving targets.

Some researchers have proposed using impulse-radio ultra-wideband (IR-UWB) radar-based methods to measure the heart rate of moving persons [15], [16]. However, their subjects moved slowly, and the experimental method was relatively simple. Furthermore, the signal energy levels that can be transmitted are not very high, which reduces the accuracy and signal-to-noise ratio (SNR) of IR-UWB radars [17]. CW Doppler radar is another common method for measuring heart rate [18]–[23]. However, owing to the lack of ranging capability in CW Doppler radar, measurements are susceptible to interference and are unsuitable for monitoring the vital signs of moving targets [24]. Therefore, an FMCW radar with good range and speed measurement capability is an appropriate choice. Furthermore, the millimeter-band FMCW radar has high sensitivity, making it easy to detect tiny displacements on the surface of the skin.

A range profile matrix (RPM)-based motion compensation method using a millimeter-wave FMCW radar has been proposed to measure the heart rate of a moving person [25], [26]. The method obtains the subject's range bin cell premise to perform position correction. If there are other objects nearby, RPM peak-seeking will have difficulty correctly selecting the range bin cell where the subject is located. In addition, the subjects' average movement speed in paper [26] was only 0.01 m/s. The authors of paper [27] proposed a method for analyzing multiple range bins simultaneously. They used a 24 GHz band radar with a low range bin resolution to cover a range of 3 m with four range bins. However, the low range bin resolution may include other nontargets in a range bin cell near the subject. Owing to the high range bin resolution of millimeter-wave FMCW radar, hundreds of range bins must be processed simultaneously, which reduces the real-time performance of the measurement system.

Although there are many sophisticated tracking filters, the goal of this study is not to predict the target's position and tracking based on its current state. Instead, selecting a range bin based on the predicted value results in a secondary error. The key to extracting high-quality phase-change information for measuring vital signs is the quick and efficient selection of the range bin cell where the subject is located. Our previous work proposed an adaptive range bin selection method for millimeter-wave FMCW radar to solve the abovementioned
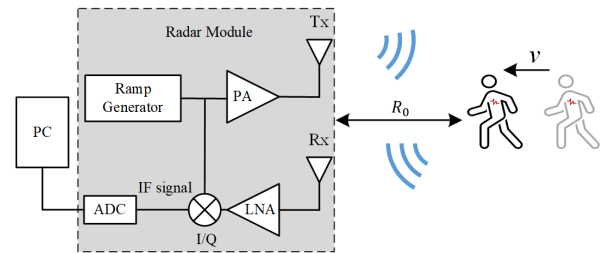
FIGURE 1. Block diagram of the FMCW radar module. The PA, LNA, and ADC represent the power amplifier, low-noise amplifier, and analog-to-digital converter, respectively. A PC was used for signal processing.
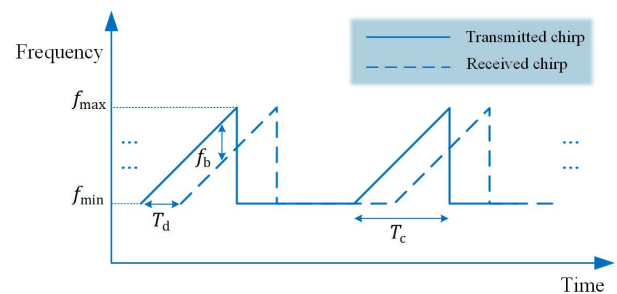
FIGURE 2. Time-frequency diagram of the transmitted and received chirps.

problem [28]. Instead of the manual post-processing form, this method automatically selects the optimal range bin cell for vital sign monitoring, and its effectiveness was demonstrated through experiments in which subjects walked back and forth in front of the radar module. Meanwhile, we proposed and evaluated methods for measuring heart rate from multiple orientations, which opens up the possibility of this research topic [29]. The adaptive range bin selection method will be improved in this study, and a comprehensive set of experimental methods will be devised to assess the accuracy and stability of the measurements. The subjects will have a maximum mean velocity of 1 m/s during the experiment and will be able to simultaneously measure the vital signs of multiple persons at the same time. Therefore, this is the first study to use FMCW radar to detect vital signs while human subjects walk at a normal speed.

Section II explains the principle of using FMCW radar to detect vital signs. The proposed method is presented in detail in Section III. Sections IV and V present experimental results and conclusions, respectively.

II. FMCW RADAR PRINCIPLE

The structure of the vital-sign measurement system based on the FMCW radar module is shown in Fig. 1. The gray area represents the radar module, which is connected to a computer that controls the radar module and performs signal processing. Fig. 2 depicts the time-frequency domain diagram of the signals transmitted and received by the radar module.

Linear upward frequency modulation was used in this study. The ramp generator periodically emits an up-chirp
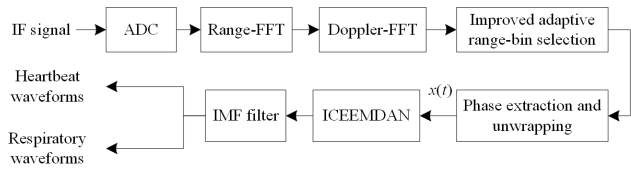
FIGURE 3. Flow chart of the proposed signal processing.

FIGURE 4. A sample of Range profile matrix (stationary vs. walking).

signal of time duration T_c at certain time intervals, with frequencies ranging from f_{min} to f_{max}. Let K_s be the slope of the frequency modulation. The sweeping bandwidth can be expressed as $B = f_{max} - f_{min} = T_c K_s$. The power amplifier amplifies the up-chirp signal. The amplified signal is then transmitted through the transmitter antenna. After the signal is reflected by various objects, the chirp signal received by the radar module is amplified by a low-noise amplifier (LNA) and correlated with the transmitted signal via the In-phase and Quadrature (I/Q) mixer, which produces the IF signal. The in-phase and quadrature components of the IF signal are then sampled separately by the ADC to generate the received complex signal and preserve its phase information, which is then processed in a PC. The IF signal can be defined as:

$$s_{if}(t) = A_t A_r \exp\left(j\left(2\pi f_{min} t_d + 2\pi K_s t_d t - \pi K_s t_d^2\right)\right),$$
$$\approx A_t A_r \exp\left(j\left(2\pi f_{min} t_d + 2\pi K_s t_d t\right)\right), t_d < t < T_c \tag{1}$$

where A_t represents the magnitude related to the transmission power, A_r is related to A_t by the radar equation, t_d is the time delay of the transmitted signal until it is received. $\pi K_s t_d^2$ in (1) can be ignored because it is small. The instantaneous distance of the measured target from the radar module R_0 versus time t_d can be expressed as:

$$R_0 = \frac{c t_d}{2}, \tag{2}$$

where c represents the speed of light. From (1) and (2), the frequency of the IF signal and its phase can be derived as follows:

$$f_b = \frac{2K_s R_0}{c}, \quad \varphi(t) = 4\pi f_{min} \frac{(R_0 + x(t))}{c}, \tag{3}$$

where $x(t)$ in this study can be interpreted as the displacement of the thoracic cavity caused by the target's heartbeat and breathing.

III. PROPOSED MEASUREMENT METHOD
A. OVERVIEW OF MEASUREMENT METHOD
A flow chart of the proposed signal processing method for vital sign measurements is shown in Fig 3. Raw data are generated in frames after the ADC samples the IF signal. The RPM can be obtained by performing a range-FFT along the fast time dimension. The change in the distance information of the target with respect to time can be observed more intuitively by stitching the RPM of each frame along the slow time dimension. The horizontal coordinates of RPM represent
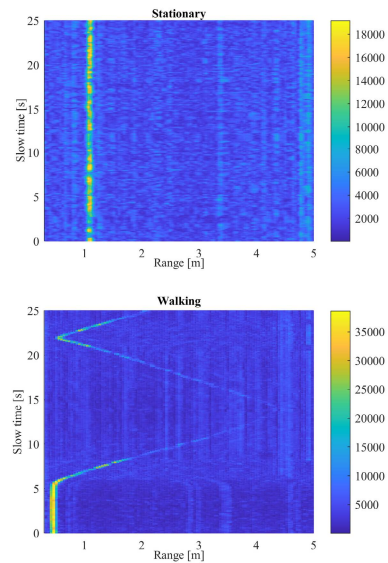
the distance to the radar module. The distance represented by each range bin cell is fixed once the radar module and its configuration file are determined.

Most previous studies on radar-based heart rate measurements required subjects to remain stationary (sitting, standing, or lying down) during the measurement. The subject was approximately 1 m from the radar module, as shown in the upper figure of Fig. 4. In this case, the range bin cell where the subject is located can be easily obtained by methods such as RPM peak finding. Moreover, once the range bin cell is identified, no adjustments are required throughout the measurement process. The phase-change information is then extracted from the most appropriate range bin cells along the time dimension, and it is unwrapped to calculate $x(t)$. By the way, in order to increase the time utilization per frame and improve the phase quality, we propose the PA-LI method of emitting multiple up-chirp signals in each frame [29]. Finally, the vital signs are typically extracted from the $x(t)$ using a band-pass filter, wavelet transform, or other means. These are the traditional radar-based vital sign measurements.

As discussed in the Introduction, there are limitations to the measurement methods mentioned above. Measurement becomes problematic when the subject walks instead of remaining stationary. As shown in the lower panel of Fig. 4, the subject walks back and forth between 0.5 m and 4.5 m from the radar module. In this case, continuous updating of the most suitable range bin cell is required to obtain the phase change information of the range bin cell where the subject is located during the measurement period. The extracted phase data are then stitched together along the time dimension.

RPM-based peak seeking is unstable because the reflected energy is lower when the subject is farther from the radar module. Even though the Doppler range matrix (DRM)-based
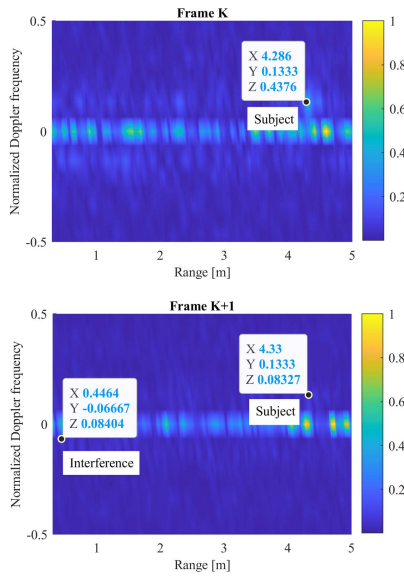
FIGURE 5. Example of Doppler-range matrix for two consecutive frames. The interval between frames is 0.1 s, and the subject is gradually moving away from the radar module.

peak-seeking method can separate the subject from most environmental noises using Doppler shift, there will probably be less energy than interference when the subject is far away. The DRM for two consecutive frames is shown in Fig. 5. For a range outside the Doppler shift of 0, frame K can identify the range bin cell where the subject is located successfully. However, for frame K+1 after 0.1s, the peak-seeking result is the range bin cell containing the interference. The result causes an error of approximately 3.89 m, and this range bin cell does not contain information about the phase change caused by the subject's skin surface displacement.

There are already some mature methods for target tracking, such as particle filters and Kalman filters. However, the goal of this study is not to improve the accuracy of the subject location and predict its position, but rather to find a simple and efficient method to identify the appropriate range bin cells and thus extract the phase change information. By contrast, overly complex algorithms can reduce the real-time performance of measurement system.

Therefore, an improved novel adaptive range bin selection method is proposed in this paper to solve the above problem. Meanwhile, this study employs the improved complete ensemble empirical mode decomposition with adaptive noise (ICEEMDAN) method to reconstruct the heartbeat and respiration signals.

B. IMPROVED ADAPTIVE RANGE BIN SELECTION METHOD

A schematic diagram of the improved adaptive range bin selection method is shown in Fig. 6. Assuming that L up-chirp signals are emitted in each frame cycle and each signal is sampled N times, each frame obtains an RPM with L rows

and N columns. A second FFT processing step is used to obtain the DRM of each frame. As an example, consider frame $K + 4$. For ease of expression, its DRM retains only the range dimension, and the scales in Fig. 6 represent the range bin cell.

The method is divided into two sections: initial position confirmation and adaptive range bin selection. In the first stage, the up-chirp signals of K frames are accumulated in a short time to obtain the initial-DRM $\boldsymbol{D}_i$. As discussed in the previous section, the data of a single frame may be disturbed by noise, and this accumulation ensures that the correct range bin cell $\alpha_{optimal}^{K}$ is acquired at the beginning of the method. In the second stage, beginning with frame $K + 1$, the peak-seeking range of the DRM for each frame is adaptively limited by the subject's instantaneous velocity, as measured by the data from the previous frames. The upper and lower limits of the peak search range and the results for frame $K + j$ are α_{max}^{K+j}, α_{min}^{K+j}, and $\alpha_{optimal}^{K+j}$, respectively ($j = 1$, 2, 3, ...J). Their relationship can be expressed as:

$$\alpha_{min}^{K+j} = \alpha_{optimal}^{K+(j-1)} - \left\lceil \frac{v_m^{K+j} T_f}{R_{bin}} \right\rceil - \beta_p^{K+j}, \quad (4)$$

$$\alpha_{min}^{K+j} = \alpha_{optimal}^{K+(j-1)} - \left\lceil \frac{v_m^{K+j} T_f}{R_{bin}} \right\rceil + \beta_p^{K+j}, \quad (5)$$

$$\beta_p^{K+j} = \left\lceil \eta \left(\frac{\alpha_{max}^{K+j} - \alpha_{min}^{K+j} + 1}{2} \right) \right\rceil, \quad (6)$$

where $\lceil \ldots \rceil$ rounds the element to the nearest integer greater than it, $\alpha_{optimal}^{K+(j-1)}$ is the index of the optimal range bin cell of the previous frame, R_{bin} denotes the length of each range bin cell. v_m^{K+j} represents the instantaneous velocity of the subject from frame K+(j-1) to the frame $K + j$. The length of the protection cell, denoted by β_p^{K+j}, is determined by the coefficient η ($0 \leq \eta \leq 1$) and the peak-seeking range. The purpose is to avoid abrupt and significant changes in the subject's velocity. Section IV describes the selection of η in detail.

Because the velocity of the subject cannot be determined until the peak search for the frame $K + j$, v_m^{K+j} can only be predicted based on previous data. In a previous study [28], the plain method was used to make v_m^{K+j} equal to the instantaneous velocity of the subject computed in the previous frame, as determined by the Doppler shift of the DRM. However, owing to measurement errors, the instantaneous speed of a given frame can fluctuate randomly. Therefore, the moving average method is used in this study to improve it.

Assuming that v_p^{K+j} represents the subject's velocity in frame $K + j$. Then, v_m^{K+j} can be expressed as

$$v_m^{K+j} = \frac{\sum_{y=1}^{Y} v_p^{K+(j-y)}}{Y}, \quad (7)$$

where Y denotes the length of the moving window. It should be noted that when Y is less than or equal to j, Y equals j.
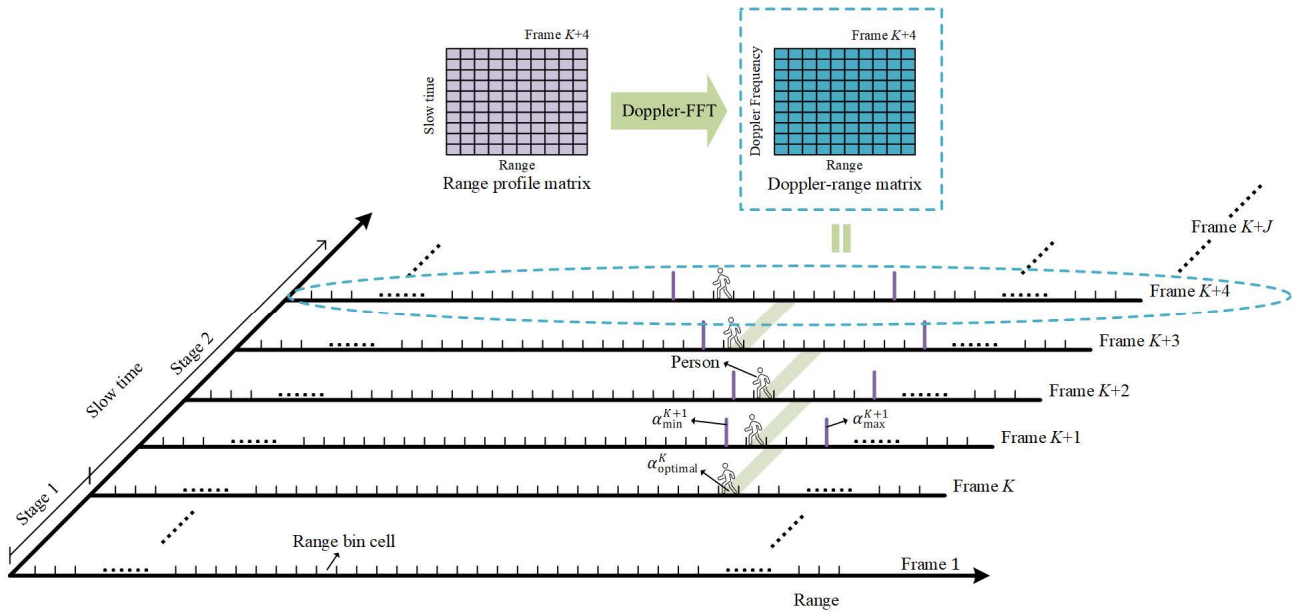
FIGURE 6. The improved adaptive range bin selection method schematic. The Doppler-range matrix of each frame is obtained by performing Doppler-FFT processing on the range profile matrix of the respective frame. The first stage of this method obtains a reliable initial range bin cell where the target is located by accumulating data. The DRM's peak-seeking range is adaptively specified from the second stage based on the target's motion.

Fig. 7 summarizes the flow of the improved adaptive range bin selection method. Because the subject is moving in this study, the phase part of (3) can be rewritten as:

$$\varphi(t) = 4\pi f_{\min} \frac{(R_0(t) + x(t))}{c}, \tag{8}$$

where $R_0(t)$ can be obtained by calculating the optimal range bin cell and R_{bin} for each frame. Therefore, $x(t)$ containing the subject's vital signs, can be calculated using (8). Furthermore, by retrieving data from the buffer at regular intervals, it is possible to control the cycle length of $x(t)$ to be measured with a specific observation window, depending on the needs of the application. In the first stage, any energy above the threshold is chosen as a valid target. If more than one valid target is detected, the phase information is saved in the buffer independently.

C. VITAL SIGNS EXTRACTION METHOD

Indeed, $x(t)$ contains not only heartbeat and respiration signals, but also body shaking and interference in the same range bin cells. There are numerous methods for extracting vital signs from $x(t)$, including band-pass filtering, wavelet transform, and EMD.

The high harmonics of the breathing signal reduce the SNR of the heartbeat signal extracted by the bandpass filter [30]. In papers [26], [31]–[36], wavelet transform was used to extract the vital signs. Because heartbeat and breathing signals differ from person to person, determining the basic function of wavelet transform is difficult. EMD can adaptively decompose a signal into a finite number of intrinsic mode functions (IMFs) based on the time scale of the signal

and then extract the desired signal based on the spectrum of each IMF [37]. However, EMD has issues with "mode mixing" and the "endpoint effect" [38], [39]. The ICEEMDAN method is an improved method based on EMD that can solve problems of the EMD and has been used to extract vital signs in our previous work [29], [40].

A flow chart of the ICEEMDAN-based vital sign extraction method is shown in Fig. 8. ICEEMDAN decomposes $x(t)$ adaptively into several IMFs and a residual $r_n(t)$, as follows:

$$x(t) = \sum_{k=1}^{n} IMF_k(t) + r_n(t), \ k = 1, 2, 3 \ldots \ldots n. \tag{9}$$

Next, FFT is performed on all IMFs and $r_n(t)$ to obtain their frequency spectrum. According to the discussion in the paper [29], the IMF filter selects the IMF with a spectrum peak appearing in the range of 0.8-2.0 Hz as the heart IMF, and the corresponding breathing IMF has a peak in the range of 0.2-0.4 Hz. They are used to reconstruct the heartbeat and respiratory signals, respectively. Targets chosen as valid in the first stage of the improved adaptive selection method are deemed invalid if the ICEEMDAN results show no heart IMF or a low SNR. In practice, the first stage is repeated regularly to refresh the valid targets. If multiple targets are in the same range bin cell, ICEEMDAN can theoretically separate their vital signs, unless their frequencies are equal.

The main goal of this study is to provide an efficient tool for the millimeter-wave FMCW radar-based vital measurement system, which allows the vital signs of moving persons to be measured. Therefore, there may be better methods to extract signals such as heartbeat from $x(t)$ in other cases, which are not discussed extensively in this paper, but the ICEEMDAN method was used to analyze the experimental results.
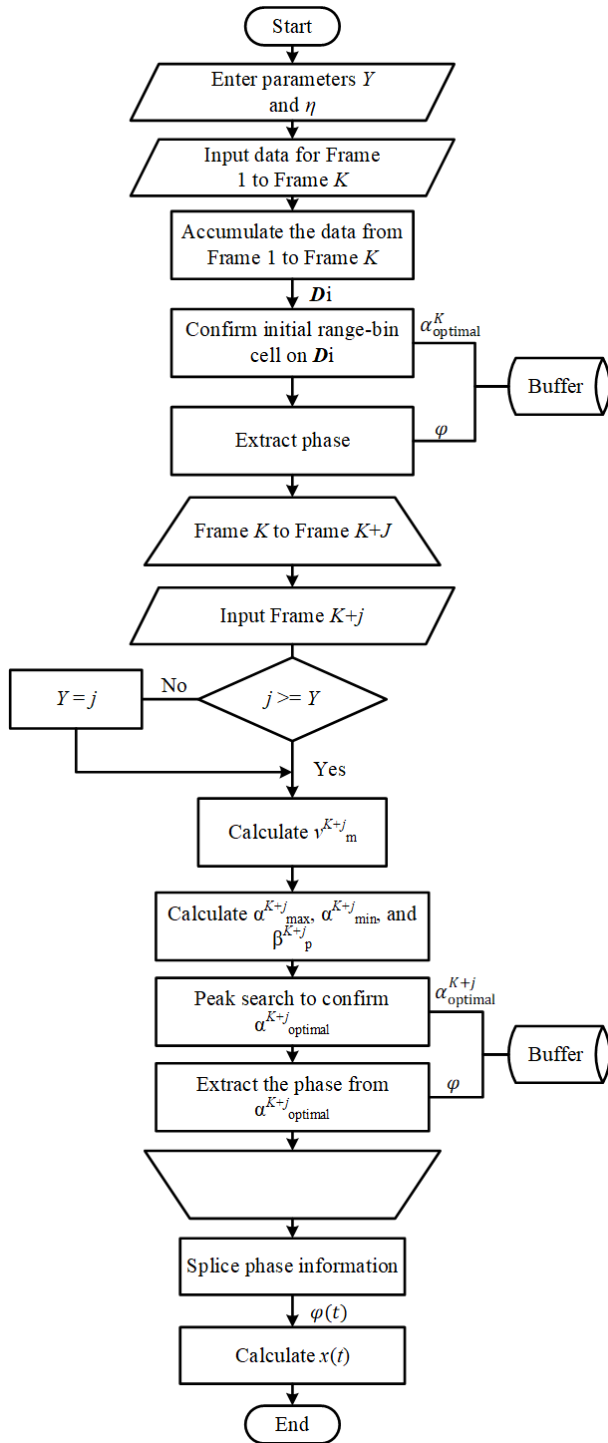
FIGURE 7. Flowchart of the improved adaptive range bin selection method.

FIGURE 8. Flow chart of vital signs extraction with ICEEMDAN.

TABLE 1. Radar module parameters.

Parameter	Value
Bandwidth	3.99 GHz
Sweep time	57 μs
Frame period	100 ms
Slope	70 MHz/μs

TABLE 2. Information about subjects.

Subject	Height [cm]	Weight [kg]
A	179	64
B	177	75
C	173	58
D	166	55
E	169	60
F	171	62
G	172	63

radiated power (EIRP) is 21 dBm, which is compliant with the FFC regulations and the Japanese Radio Law. Furthermore, it is not harmful to the human body.

This experiment included seven subjects who walked along the route shown in Fig. 9. Subjects walked at 0.5 m/s and 1 m/s on route A to demonstrate the efficacy of the proposed method. The other two routes walked at a speed of 0.5 m/s. Furthermore, the subjects wore electrocardiography (ECG) equipment to measure their ECG and heart rate.

Fig. 10 depicts the actual experimental scenario, whereas Fig. 9 depicts a hypothetical space designed to better understand why walking on such a route is desirable. This measurement system is not limited to living rooms; it can also be used in wards, nursing homes, and rehabilitation rooms, and other places. Table 2 lists the height and weight of each experimental participant.

IV. EXPERIMENT

A. EQUIPMENT AND EXPERIMENT ENVIRONMENT

The radar module used in this study is based on the Texas Instruments Inc. IWR1443, which operates at frequencies ranging from 77 GHz to 81 GHz. Table 1 lists the main parameters of the radar module. The maximum effective isotropic
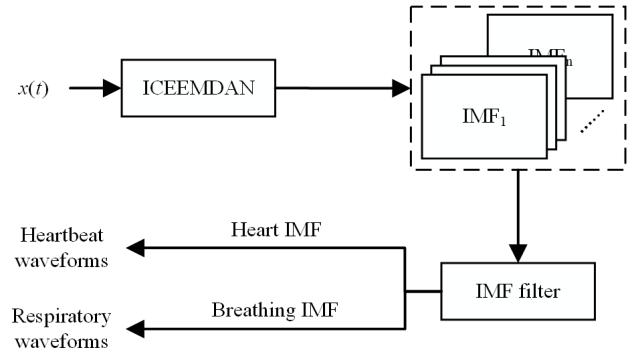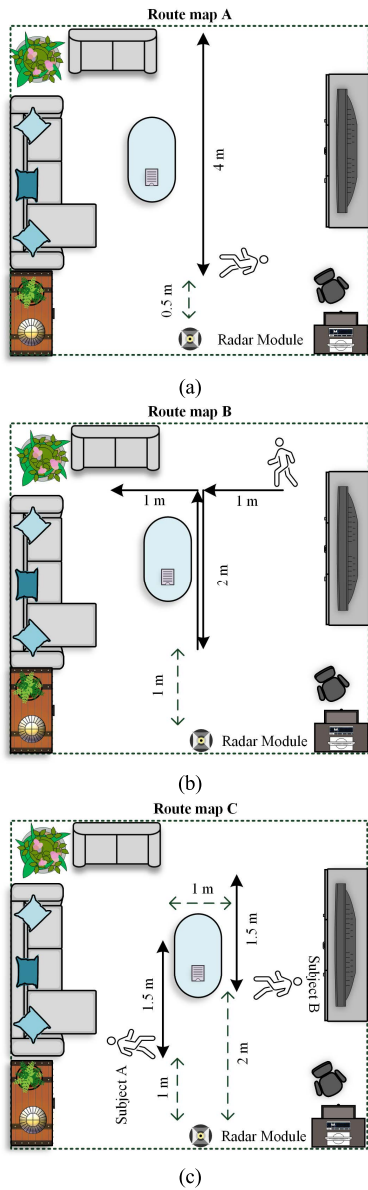
B. PARAMETER ANALYSIS

Parameter K is related to the accuracy of the initial range bin cell, but is inversely proportional to real-time performance of

FIGURE 9. Walking route maps of subjects. Route map A: The subject moves back and forth between 0.5 m and 4.5 m from the radar module at speeds of 0.5 m/s and 1 m/s. Route map B: The subject walks at 0.5 m/s in the direction of the arrow on the map. Route map C: At 1 m and 2 m from the radar module, both subjects walked back and forth at a speed of 0.5 m/s.

FIGURE 10. Experimental scenario for route C.

the measurement system. K was set to 5 in this experiment, implying that the first stage of the improved adaptive range bin selection method takes 0.5 s.

Parameter η is related to the maximum allowable speed increment per second. This experiment has a frame duration of 0.1 seconds, and when η is set to 0.1, the maximum speed increments per second allowed for initial speeds of 0.5 m/s and 1 m/s is 1.18 m/s and 2.36 m/s, respectively. Since most of the audience for this measurement system are older people and patients undergoing rehabilitation, who typically walk indoors at speeds of no more than 1 m/s, η was set to 0.1.

Parameter η can be adjusted flexibly based on the application scenario and environment. Furthermore, v_m^{K+j} denotes the relative velocity of a subject in the radar module. Even if the subject is not directly in front of the radar, the value decreases after converting to the relative velocity, indicating that the optimal range bin cell is not outside the range of peak-seeking.

Parameter Y was set to 5 to reduce the error that occurs when measuring the subject's instantaneous velocity through a single frame. This implies that v_m^{K+j} was calculated based on the velocity of the subject during the previous 0.5 s. As previously discussed, the variation in the speed of the subjects is not significant, so Y does not need to be set too high.

C. EXPERIMENT RESULTS
1) FIXED-ROUTE EXPERIMENTS
The measurement period for routes B and C was 20 s, and the measurement period for route A was 32 s to ensure at least three back-and-forth walks. For simplicity, the two cases of route A are referred to as route A1 (mean speed of 0.5 m/s) and route A2 (mean speed of 1 m/s). Fig. 11 depicts the optimal range bin selection results obtained by the RPM peak-seeking method, RDM peak-seeking method, and proposed method. This figure shows the results for routes A1, A2, B, and C, from top to bottom.

As discussed in the introduction and Section III of this paper, motion compensation based on either RPM or RDM peak-seeking is unstable in either case. The results show that the optimal range bin variations obtained by RPM and RDM peak-seeking are disturbed, resulting in significant random jitter.

The overall accuracy of the optimal range bin selection based on RPM peak-seeking was less than 40% at 31.7%. In particular, the worst performance was observed for route A2, where the average speed was high.

The accuracy of RDM-based peak seeking was 82.8% and 88.3% in the case of routes A1 and A2, respectively. However, there is still a significant jitter across the distance. The results for route B demonstrate the limitations of the method when the subjects walk horizontally. Furthermore, in the case of
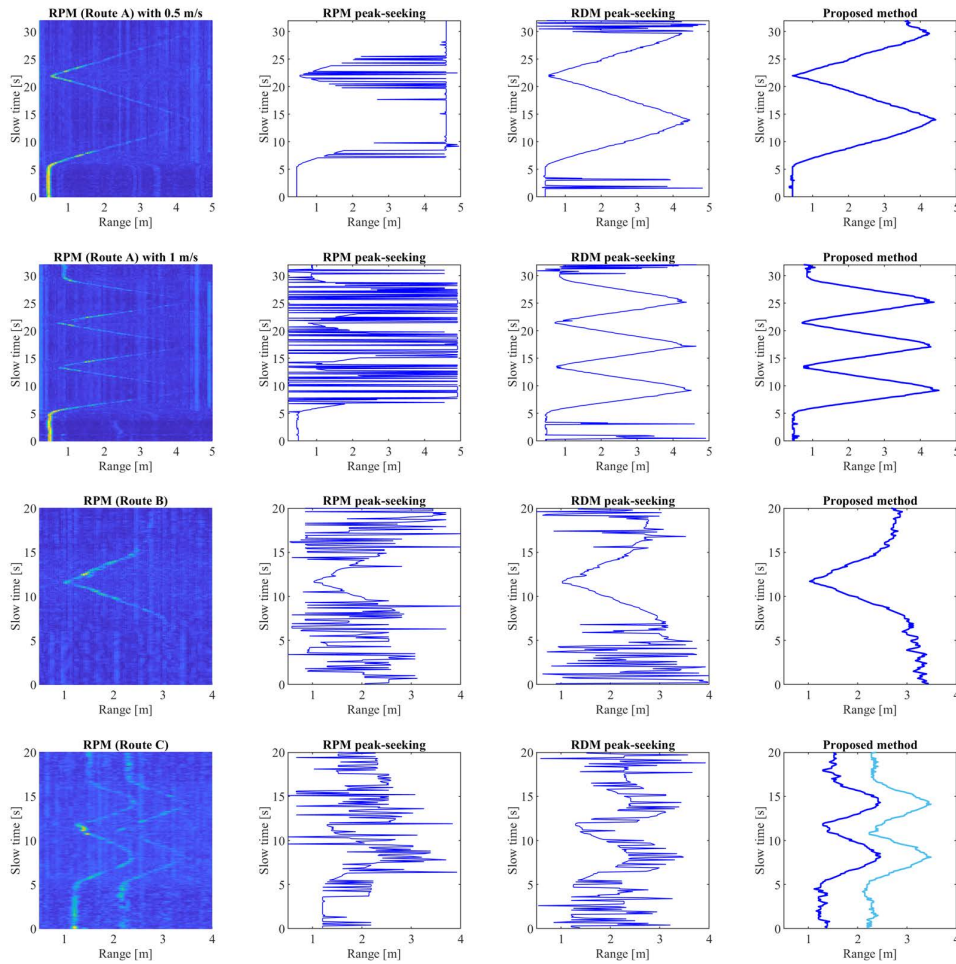
FIGURE 11. Results of range bin cell selection. From top to bottom, the diagram shows the results for route A (with a mean speed of 0.5 m/s), route A (with a mean speed of 1 m/s), route B, and route C.

route C, the range bin selections of the two subjects interfered with each other.

The improved adaptive range bin selection method proposed in this study can solve the problems associated with comparison methods. In the case of routes A1 and A2, the accuracy of the range bin cells obtained using the proposed method was 97.8% and 94.7%, respectively. Route B shows that even when the subject faces the radar module sideways, the range bin cell can be accurately identified. Most importantly, the first stage of the proposed method can identify multiple trackable targets, allowing the vital signals of multiple moving targets to be simultaneously measured.

Because route B is more complex than the other routes, the results of $x(t)$ signal decomposition by ICEEMDAN are shown in Fig. 12 to demonstrate the effectiveness of the proposed method. This observation window lasted 20 s, and the spectrum analysis revealed that IMF_2 and IMF_4 were the heart IMF and breathing IMF, respectively. Furthermore, this heart IMF has a high SNR with a significant peak to aid in the measurement of the heart rate and will reconstruct the heartbeat signal. The respiratory signal is simple to measure owing to its high amplitude and low frequency. Therefore,
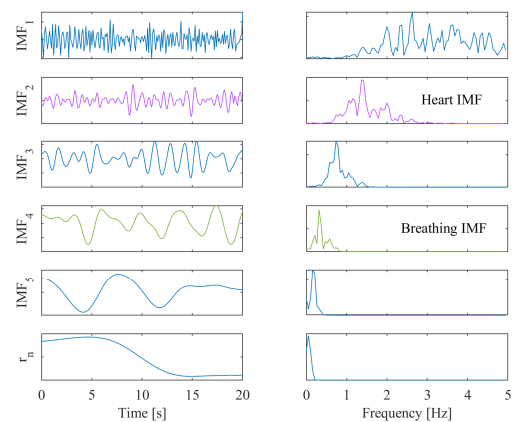
FIGURE 12. Results of ICEEMDAN decomposition. The left and right sides are the time domain and frequency domain, respectively. The $x(t)$ signal is obtained by the proposed method and is in the case of route B.

the measurement of the heartbeat signal is the focus of this study.

As shown in Fig. 13, the heartbeat signals measured by the two comparison methods and the proposed method are
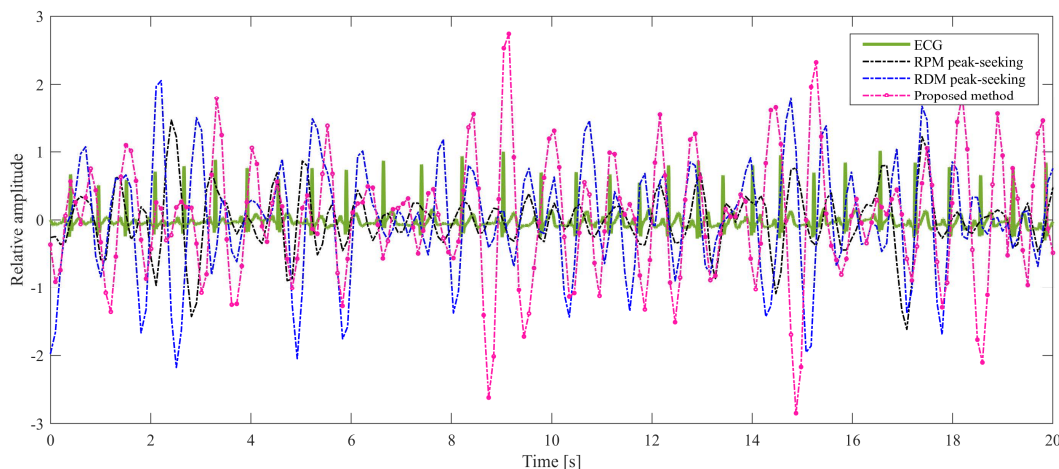
FIGURE 13. The reconstructed heartbeat waveforms versus ECG waveform in the time domain.

compared to the ECG signal. The heartbeat waveforms reconstructed by the comparison methods correlated poorly with the ECG signals. The RR interval of the heartbeat waveform acquired using the proposed method, on the other hand, remained highly consistent with that of the ECG signal even when the subject walked laterally for period of 0-6 s and 15-20 s. At the same time, data from this observation window revealed that the heartbeat waveform fluctuated slightly when the subject turned, but the overall heart rate error was only 2.01 bpm compared to the ECG signal.

Table 3 displays the results of the heart rate measurements for each route condition, with the measured values and absolute errors in beats per minute (bpm). Subjects A, C, E, and G walked in the 2-3.5 m range in the route C experiment, while subjects B, D, and F walked in the 1-2.5 m range. The results showed that the accuracy of the RPM peak-seeking method in measuring the heart rate was poor and almost lost its referential value. The RDM peak-seeking method improves the accuracy of the heart rate measurement over the former method, but it is precarious and unreliable. In the case of routes A1, A2, B, and C, the mean absolute errors of heart rate measured by the proposed method were 3.11 bpm, 3.10 bpm, 3.47 bpm, and 5.24 bpm, with an overall root mean squared error (RMSE) of 4.09 bpm. In paper [26], the subjects moved very slowly and had a heart rate estimation accuracy of 90%. As in the previous study, the subjects in [15] performed only backward and forward movements at a slow speed with a measurement error range of 0-8 bpm. The authors of paper [16] used multiple radars to measure the heart rate of a moving target with an accuracy of about 86%. The mean heart rate measurement accuracy of the proposed method was 95.88%. The results for routes A1 and A2 show that even accelerating the walking speed to 1 m/s does not reduce the accuracy of the measurement results. Furthermore, the experimental results for routes B and C fully demonstrate the validity and application potential of the proposed measurement method.
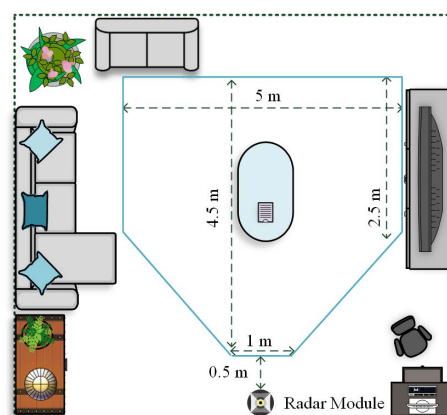

FIGURE 14. The environment for the random walk experiment is depicted in this diagram.

2) RANDOM WALK EXPERIMENTS

Two subjects walked randomly and simultaneously in the area depicted in Fig. 14 at speeds ranging from 0 to 1 m/s for 10 minutes. The area is approximately 18.5 square meters, comparable to a typical bedroom or living room.

The 10-minute streaming data was analyzed using a 20-second observation window and a 1-second sliding step because route C of the fixed-route tests had a measurement period of 20 seconds. There were 581 observation windows data for each subject for the measurement time. Fig. 15 shows the absolute error distributions of the heart rates obtained by each window measurement compared to the corresponding ECG data. The findings of this experiment demonstrate that the vast majority of absolute errors fall between the 0 to 5 bpm range, which is consistent with the results of previous fixed-route tests. Due to the right side of the human body facing the radar for a long time or a large body shake when turning, a small number of observation windows showed an absolute error of more than 5 bpm.

TABLE 3. Heart rate measurement results (Measured value: [bpm], Absolute error: [bpm]).

Route	Subject	ECG	RPM peak-seeking		RDM peak-seeking		Proposed method		
			Measured value	Absolute error	Measured value	Absolute error	Measured value	Absolute error	Accuracy
A1	A	92.76	73.14	19.62	101.28	8.52	88.14	4.62	95.02%
	B	94.38	61.86	32.52	67.50	26.88	90.00	4.38	95.36%
	C	87.84	61.96	25.88	67.52	20.32	90.02	2.18	97.52%
	D	115.14	65.64	49.50	82.50	32.64	112.50	2.64	97.71%
	E	82.68	99.36	16.68	76.86	5.82	84.36	1.68	97.97%
	F	76.86	84.36	7.50	72.13	4.73	73.14	3.72	95.16%
	G	76.20	80.64	4.44	73.14	3.06	78.78	2.58	96.61%
A2	A	99.00	80.64	18.36	86.28	12.72	101.28	2.28	97.70%
	B	98.22	90.00	8.22	101.29	3.07	100.23	2.01	97.95%
	C	99.96	69.36	30.60	82.51	17.45	97.50	2.46	97.54%
	D	105.96	86.27	19.69	88.17	17.79	103.14	2.82	97.34%
	E	80.14	69.50	10.64	73.41	6.73	76.92	3.22	95.98%
	F	93.60	78.78	14.82	101.28	7.68	88.68	4.92	94.74%
	G	84.00	73.17	10.83	93.78	9.78	88.01	4.01	95.23%
B	A	100.98	75.00	25.98	93.75	7.23	95.50	5.48	94.57%
	B	93.12	101.25	8.13	84.38	8.74	99.38	6.26	93.28%
	C	92.28	75.00	17.28	78.75	13.53	88.13	4.15	95.50%
	D	115.38	65.63	49.75	108.76	6.62	116.25	0.87	99.25%
	E	88.26	84.36	3.90	99.36	11.10	86.25	2.01	97.72%
	F	79.56	67.50	12.06	66.00	13.56	84.36	4.80	93.97%
	G	85.08	90.00	4.92	82.50	2.58	84.36	0.72	99.15%
C	A	91.38	80.64	10.74	84.36	7.02	95.64	4.26	95.34%
	B	97.44	76.86	20.58	105.00	7.56	93.78	3.66	96.24%
	C	91.74	80.63	11.11	82.50	9.24	99.36	7.62	91.69%
	D	109.80	75.00	34.80	93.78	16.02	103.14	6.66	93.93%
	E	91.20	71.28	19.92	67.50	23.70	86.28	4.92	94.61%
	F	75.90	105.00	29.10	86.28	10.38	80.64	4.74	93.75%
	G	77.94	67.50	10.44	95.64	17.70	73.14	4.80	93.84%
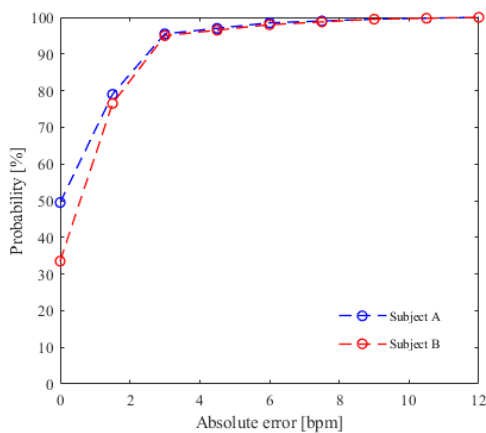
FIGURE 15. The results of a random walk experiment's heart rate measurements. The absolute errors between the measured values and the ECG data are presented in the form of cumulative distribution functions.

Overall, the proposed method's measurement error is within acceptable limits. This experiment proved the stability of the method.

V. CONCLUSION

In conclusion, this study proposes a novel FMCW radar-based vital sign monitoring method for moving persons. The proposed improved adaptive range bin selection method efficiently selects the optimal range bin cells to obtain high-quality phase-change information, and the reconstructed heartbeat signal using the ICEEMDAN method is highly consistent with the ECG signal. The overall RMSE for heart rate estimation was 4.09 bpm, with an accuracy of 95.88%. The experimental results showed that the accuracy of the heart rate measurement remained high regardless of whether the subjects walked at 1 m/s or with the left side of their body facing the radar. Furthermore, random walk experiments have proved its good stability. Therefore, this measurement method has application potential. Measuring vital signs from the right side of the human body is challenging, and there is a classification problem if multiple targets are in the same range bin cell for an extended period. Therefore, we plan to use multiple radars to improve this measurement system in future studies.

REFERENCES

[1] P. Mehrgardt, M. Khushi, S. Poon, and A. Withana, "Deep learning fused wearable pressure and PPG data for accurate heart rate monitoring," *IEEE Sensors J.*, vol. 21, no. 23, pp. 27106–27115, Dec. 2021.

[2] D. Biswas, L. Everson, M. Liu, M. Panwar, B. Verhoef, S. Patki, C. H. Kim, A. Acharyya, C. V. Hoof, M. Konijnenburg, and N. V. Helleputte, "Cor-NET: Deep learning framework for PPG-based heart rate estimation and biometric identification in ambulant environment," *IEEE Trans. Biomed. Circuits Syst.*, vol. 13, no. 2, pp. 282–291, Apr. 2019.

[3] E. Grooby, J. He, J. Kiewsky, D. Fattahi, L. Zhou, A. King, A. Ramanathan, A. Malhotra, G. A. Dumont, and F. Marzbanrad, "Neonatal heart and lung sound quality assessment for robust heart and breathing rate estimation for telehealth applications," *IEEE J. Biomed. Health Informat.*, vol. 25, no. 12, pp. 4255–4266, Dec. 2021.

[4] H. Zhao, H. Hong, L. Sun, Y. Li, C. Li, and X. Zhu, "Noncontact physiological dynamics detection using low-power digital-IF Doppler radar," *IEEE Trans. Instrum. Meas.*, vol. 66, no. 7, pp. 1780–1788, Jul. 2017.

[5] S. M. Sharpe, J. Seals, A. H. MacDonald, and S. R. Crowgey, "Non-contact vital signs monitor," U.S. Patent 4 958 638, Sep. 25, 1990.

[6] O. B. Lubecke, P.-W. Ong, and V. M. Lubecke, "10 GHz Doppler radar sensing of respiration and heart movement," in *Proc. IEEE 28th Annu. Northeast Bioeng. Conf.*, Philadelphia, PA, USA, Apr. 2002, pp. 55–56.

[7] T. Sakamoto, P. J. Aubry, S. Okumura, H. Taki, T. Sato, and A. G. Yarovoy, "Noncontact measurement of the instantaneous heart rate in a multi-person scenario using X-band array radar and adaptive array processing," *IEEE J. Emerg. Sel. Topics Circuits Syst.*, vol. 8, no. 2, pp. 280–293, Jun. 2018.

[8] M. Alizadeh, G. Shaker, J. C. M. De Almeida, P. P. Morita, and S. Safavi-Naeini, "Remote monitoring of human vital signs using mm-wave FMCW radar," *IEEE Access*, vol. 7, pp. 54958–54968, 2019.

[9] D. Yang, Z. Zhu, and B. Liang, "Vital sign signal extraction method based on permutation entropy and EEMD algorithm for ultra-wideband radar," *IEEE Access*, vol. 7, pp. 178879–178890, 2019.

[10] A. Ahmad, J. C. Roh, D. Wang, and A. Dubey, "Vital signs monitoring of multiple people using a FMCW millimeter-wave sensor," in *Proc. IEEE Radar Conf. (RadarConf)*, Oklahoma City, OK, USA, Apr. 2018, pp. 1450–1455.

[11] W. Lv, Y. Zhao, W. Zhang, W. Liu, A. Hu, and J. Miao, "Remote measurement of short-term heart rate with narrow beam millimeter wave radar," *IEEE Access*, vol. 9, pp. 165049–165058, 2021.

[12] S. Wang, A. Pohl, T. Jaeschke, M. Czaplik, M. Köny, S. Leonhardt, and N. Pohl, "A novel ultra-wideband 80 GHz FMCW radar system for contactless monitoring of vital signs," in *Proc. IEEE 37th Annu. Int. Conf. Eng. Med. Biol. Soc. (EMBC)*, Milan, Italy, Aug. 2015, pp. 4978–4981.

[13] K.-K. Shyu, L.-J. Chiu, P.-L. Lee, T.-H. Tung, and S.-H. Yang, "Detection of breathing and heart rates in UWB radar sensor data using FVPIEF-based two-layer EEMD," *IEEE Sensors J.*, vol. 19, no. 2, pp. 774–784, Jan. 2019.

[14] T. Sakamoto, M. Muragaki, K. Tamura, S. Okumura, T. Sato, K. Mizutani, K. Inoue, T. Fukuda, and H. Sakai, "Measurement of instantaneous heart rate using radar echoes from the human head," *Electron. Lett.*, vol. 54, no. 14, pp. 864–866, Dec. 2018.

[15] Y. Rong, K. V. Mishra, and D. W. Bliss, "Multiple moving targets heartbeat estimation and recovery using multi-frequency radars," in *Proc. IEEE Radar Conf. (RadarConf)*, May 2021, pp. 1–5.

[16] X. Yang, X. Zhang, H. Qian, Y. Ding, and L. Zhang, "MMT-HEAR: Multiple moving targets heartbeats estimation and recovery using IR-UWB radars," in *Proc. 42nd Annu. Int. Conf. IEEE Eng. Med. Biol. Soc. (EMBC)*, Jul. 2020, pp. 5733–5736.

[17] G. Wang, J.-M. Muñoz-Ferreras, C. Gu, C. Li, and R. Gómez-García, "Application of linear-frequency-modulated continuous-wave (LFMCW) radars for tracking of vital signs," *IEEE Trans. Microw. Theory Techn.*, vol. 62, no. 6, pp. 1387–1399, Jun. 2014.

[18] V. L. Petrović, M. M. Janković, A. V. Lupšić, V. R. Mihajlović, and J. S. Popović-Božović, "High-accuracy real-time monitoring of heart rate variability using 24 GHz continuous-wave Doppler radar," *IEEE Access*, vol. 7, pp. 74721–74733, 2019.

[19] J.-H. Park, Y.-J. Jeong, G.-E. Lee, J.-T. Oh, and J.-R. Yang, "915-MHz continuous-wave Doppler radar sensor for detection of vital signs," *Electronics*, vol. 8, no. 5, p. 561, May 2019.

[20] H.-R. Chuang, H.-C. Kuo, F.-L. Lin, T.-H. Huang, C.-S. Kuo, and Y.-W. Ou, "60-GHz millimeter-wave life detection system (MLDS) for noncontact human vital-signal monitoring," *IEEE Sensors J.*, vol. 12, no. 3, pp. 602–609, Mar. 2012.

[21] M. Sekine and K. Maeno, "Non-contact heart rate detection using periodic variation in Doppler frequency," in *Proc. IEEE Sensors Appl. Symp.*, Feb. 2011, pp. 318–322.

[22] M. Mercuri, Y. Liu, I. Lorato, T. Torfs, F. Wieringa, A. Bourdoux, and C. V. Hoof, "A direct phase-tracking Doppler radar using wavelet independent component analysis for non-contact respiratory and heart rate monitoring," *IEEE Trans. Biomed. Circuits Syst.*, vol. 12, no. 3, pp. 632–643, Jun. 2018.

[23] N. T. P. Nguyen, P.-Y. Lyu, M. H. Lin, C.-C. Chang, and S.-F. Chang, "A fshort-time autocorrelation method for noncontact detection of heart rate variability using CW Doppler radar," in *IEEE MTT-S Int. Microw. Symp. Dig.*, May 2019, pp. 1–4.

[24] G. Wang, C. Gu, T. Inoue, and C. Li, "A hybrid FMCW-interferometry radar for indoor precise positioning and versatile life activity monitoring," *IEEE Trans. Microw. Theory Techn.*, vol. 62, no. 11, pp. 2812–2822, Nov. 2014.

[25] M. Shibao and A. Kajiwara, "Heart-rate monitoring of moving persons using 79 GHz ultra-wideband radar sensor," *IEICE Commun. Exp.*, vol. 9, no. 5, pp. 125–130, 2020.

[26] A. Morimatsu, S. Matsuguma, and A. Kajiwara, "Heart rate estimation of a moving person using 79 GHz-band UWB radar," in *Proc. IEEE Sensors Appl. Symp. (SAS)*, Sophia Antipolis, France, Mar. 2019, pp. 1–5.

[27] I. Nejadgholi, S. Rajan, and M. Bolic, "Time-frequency based contactless estimation of vital signs of human while walking using PMCW radar," in *Proc. IEEE 18th Int. Conf. e-Health Netw., Appl. Services (Healthcom)*, Munich, Germany, Sep. 2016, pp. 1–6.

[28] Y. Hu and T. Toda, "A novel adaptive range-bin selection method for remote heart-rate measurement of an indoor moving person using mm-wave FMCW radar," *IEICE Commun. Exp.*, vol. 10, no. 5, pp. 277–282, May 2021.

[29] Y. Hu and T. Toda, "The effect of multi-directional on remote heart rate measurement using PA-LI joint ICEEMDAN method with mm-wave FMCW radar," *IEICE Trans. Commun.*, vol. E105.B, no. 2, pp. 159–167, Feb. 2022.

[30] D. R. Morgan and M. G. Zierdt, "Novel signal processing techniques for Doppler radar cardiopulmonary sensing," *Signal Process.*, vol. 89, no. 1, pp. 45–66, Jan. 2009.

[31] T. K. V. Dai, Y. Yu, P. Theilmann, A. E. Fathy, and O. Kilic, "Remote vital sign monitoring with reduced random body swaying motion using heartbeat template and wavelet transform based on constellation diagrams," *IEEE J. Electromagn., RF Microw. Med. Biol.*, early access, Jan. 25, 2022.

[32] S. Sato, Y. Hu, and T. Toda, "A study of multi-directional heart-rate-estimation with discrete wavelet transform and band pass filter with 77 GHz-band FMCW radar," in *Proc. IEICE 1st Int. Conf. Emerg. Technol. Commun. (ICETC)*, Dec. 2020, pp. 1–4.

[33] M. P. Ebrahim, F. Heydari, J.-M. Redoute, and M. R. Yuce, "Accurate heart rate detection from on-body continuous wave radar sensors using wavelet transform," in *Proc. IEEE SENSORS*, Oct. 2018, pp. 1–4.

[34] M. Li and J. Lin, "Wavelet-transform-based data-length-variation technique for fast heart rate detection using 5.8-GHz CW Doppler radar," *IEEE Trans. Microw. Theory Techn.*, vol. 66, no. 1, pp. 568–576, Jan. 2018.

[35] A. Tariq, A. Zahid, U. Khan, N. Khan, and F. Khan, "Implementation of wavelet transform for monitoring of vital signs through IR-UWB radar," in *Proc. Int. Conf. Commun., Comput. Digit. Syst. (C-CODE)*, Mar. 2017, pp. 337–340.

[36] X. Liang, H. Zhang, T. Lyu, L. Xu, C. Cao, and T. A. Gulliver, "Ultra-wide band impulse radar for life detection using wavelet packet decomposition," *Phys. Commun.*, vol. 29, pp. 31–47, Aug. 2018.

[37] N. E. Huang, Z. Shen, S. R. Long, M. L. C. Wu, H. H. E. Shih, Q. Zheng, N. C. Yen, C. Tung, and H. H. Liu, "The empirical mode decomposition and the Hilbert spectrum for nonlinear and non-stationary time series analysis," *Proc. Roy. Soc. London A, Math., Phys. Eng. Sci.*, vol. 454, no. 1971, pp. 903–995, Mar. 1998.

[38] Z. Wu and N. E. Huang, "Ensemble empirical mode decomposition: A noise-assisted data analysis method," *Adv. Adapt. Data Anal.*, vol. 1, no. 1, pp. 1–41, 2009.

[39] M. E. Torres, M. A. Colominas, G. Schlotthauer, and P. Flandrin, "A complete ensemble empirical mode decomposition with adaptive noise," in *Proc. IEEE Int. Conf. Acoust., Speech Signal Process. (ICASSP)*, Prague, Czech Republic, Jul. 2011, pp. 4144–4147.

[40] M. A. Colominas, G. Schlotthauer, and M. E. Torres, "Improved complete ensemble EMD: A suitable tool for biomedical signal processing," *Biomed. Signal Process. Control*, vol. 14, pp. 19–29, Nov. 2014.

TAKESHI TODA received the B.E. degree in electrical engineering from Nihon University, Tokyo, Japan, in 1992, the M.S. degree in electronic engineering from the University of Electro-Communications, Tokyo, in 1994, and the D.E. degree from the Tokyo Institute of Technology, Tokyo, in 2004. From 1994 to 2004, he worked at Fujitsu Laboratories Ltd., Kawasaki, Japan. From 2004 to 2005, he worked at eAccess Ltd., Tokyo. From 2005 to 2008, he worked at the Kyocera Corporation, Research and Development Center, Yokohama, Japan. He is currently a Professor with the College of Science and Technology, Nihon University, Tokyo. His current research interests include radar signal processing, machine learning, and system-information engineering. He is a member of the Institute of Electronics, Information and Communication Engineers (IEICE).

● ● ●

YAOKUN HU received the B.E. degree in electrical engineering and automation from the Hunan Institute of Engineering, China, in 2017, and the M.E. degree in electrical engineering from Nihon University, Japan, in 2021, where he is currently pursuing the Ph.D. degree in electrical engineering with the Graduate School of Science and Technology. He joined at Fujitsu Ltd., Japan, in 2021, where he is working in research and development. His current research interests include radar signal processing, biomedical signal processing, and machine learning. He is a member of the Institute of Electronics, Information and Communication Engineers (IEICE) of Japan.